Research Article | Open Access

Chemical Synthesis

Xu et al. Chem. Synth. 2026, 6, 70 DOI:10.20517/cs.2025.92

Halogen termination engineering of Mo_2CT_x MXenes for high-capacitance supercapacitors via electronegativity modulation

Hanchen Xu[1,#], Hongwei Shou[1,#], Quan Zhou[1], Hengjie Liu[1], Shiqiang Wei[1], Xiaojun Wu[2,*], Changda Wang[1,*], Li Song[1,3,*]

Keywords:
Halogen surface terminations, electrochemical double-layer, MXenes energy storage, capacitance regulation mechanism

Citation: Xu, H.; Shou, H.; Zhou, Q.; Liu, H.; Wei, S.; Wu, X.; Wang, C.; Song, L. Halogen termination engineering of Mo_2CT_x MXenes for high-capacitance supercapacitors via electronegativity modulation. *Chem. Synth.* **2026**, *6*, 70. https://dx.doi.org/10.20517/cs.2025.92

Received: 21 Aug 2025 **First Decision:** 26 Dec 2025 **Revised:** 5 Jan 2026 **Accepted:** 28 Jan 2026 **Published:** 21 Aug 2026

Academic Editor: Ying Wan
Copy Editor: Pei-Yun Wang
Production Editor: Pei-Yun Wang

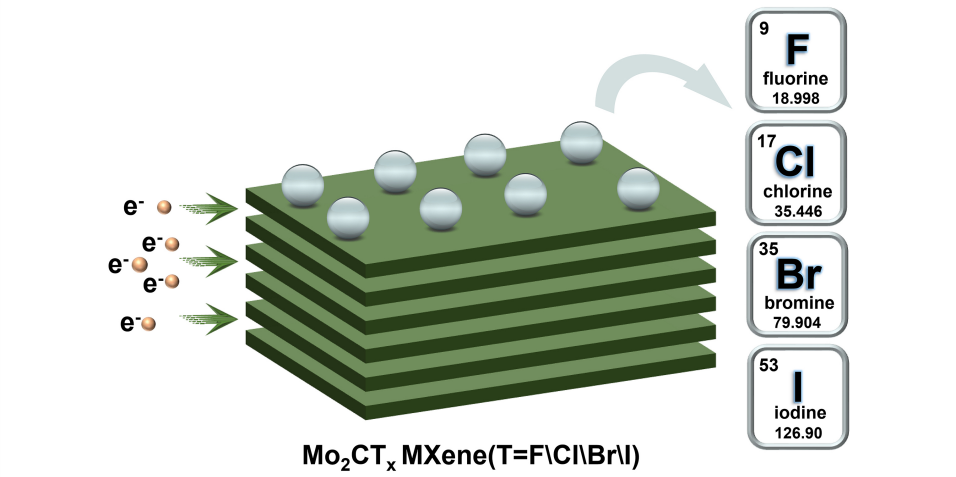

Abstract

The electrochemical performances of MXenes (transition metal carbides/nitrides) are critically governed by their surface terminations, yet the role of halogen electronegativity in modulating capacitive behavior remains underexplored. Here, we demonstrate through integrated density functional theory calculations and experimental validation that tailored halogen terminations (F, Cl, Br, I) on Mo_2CT_x MXenes directly regulate their electric double-layer capacitance. Computational analysis reveals that lower electronegativity terminations reduce electrostatic shielding, thinning the double-layer interface and enhancing charge storage, yielding a capacitance hierarchy: Mo_2CF_x (9.23 μF/cm²) < Mo_2CCl_x (10.10 μF/cm²) < Mo_2CBr_x (11.30 μF/cm²) < Mo_2CI_x (12.96 μF/cm²). Experimentally, solvothermal halogen substitution (HCl/HBr/HI) produces termination-specific Mo_2CT_x with retained crystallinity and controlled surface chemistry. Electrochemical measurements in 1 M H_2SO_4 confirm that I-terminated Mo_2CT_x achieves a

[1]National Synchrotron Radiation Laboratory, CAS Center for Excellence in Nanoscience, University of Science and Technology of China, Hefei 230029, Anhui, China.
[2]CAS Key Laboratory for Materials for Energy Conversion, School of Chemistry and Materials Science, Synergetic Innovation of Quantum Information & Quantum Technology, University of Science and Technology of China, Hefei 230026, Anhui, China.
[3]Zhejiang Institute of Photonelectronics, Jinhua 321004, Zhejiang, China.
[#]Authors contributed equally to this work.

[*]**Correspondence to:** Prof. Xiaojun Wu, CAS Key Laboratory for Materials for Energy Conversion, School of Chemistry and Materials Science, Synergetic Innovation of Quantum Information & Quantum Technology, University of Science and Technology of China, Hefei 230026, Anhui, China. E-mail: xjwu@ustc.edu.cn; Prof. Changda Wang, Prof. Li Song, National Synchrotron Radiation Laboratory, CAS

Center for Excellence in Nanoscience, University of Science and Technology of China, Hefei 230029, Anhui, China. E-mail: wchda@ustc.edu.cn; song2012@ustc.edu.cn

specific capacitance of 539.3 F/g at 1 A/g, 2.16 times higher than F-terminated counterparts, with exception rate retention (> 30% at 100 mV/s). This performance stems from I-termination's dual role, enlarging interlayer spacing for enhanced ion accessibility and increasing surface electron density on Mo atoms, as evidenced by differential charge density analysis. These findings provide a rational design strategy for MXene-based supercapacitors through precise surface termination control, bridging atomic-scale insights to macroscopic energy storage applications.

INTRODUCTION

Two-dimensional transition metal carbides/nitrides (MXenes) have emerged as promising electrode materials for electric double layer capacitors (EDLCs) due to their layered structures, high specific surface area, high conductivity, tunable surface chemistry and high specific capacitance (> 300 F/g)[1-4]. In the general formula of MXenes ($M_{n+1}X_nT_x$), "M" represents a transition metal, "X" is carbon or nitrogen, and "T_x" denotes surface termination. Their capacitance arises from dual mechanisms: electric double-layer (EDL) charge storage facilitated by accessible interlayer spaces and pseudo-capacitive contributions from redox-active surface terminations (e.g., -O, -OH)[5,6]. Notably, the surface terminations (T) that directly contact the electrolyte have a significant impact on the capacitance of MXene electrodes[7-9]. However, conventional synthesis routes, such as hydrofluoric acid (HF) etching, introduce inert fluorine terminations, which limit capacitance (< 100 F/g) due to suppressed ion accessibility and redox activity. In contrast, fluoride-free methods [e.g., LiF/hydrochloric acid (HCl) or HF/LiCl etching] yield MXenes with Cl terminations and higher capacitances (> 200 F/g)[10,11], highlighting the critical role of surface chemistry in modulating electrochemical performance[12].

Recent advances in MXenes synthesis, including molten salt etching and hydrothermal processing, enable precise control over surface terminations (e.g., -O/-S, -Cl, -Br, -I, -BrI, -ClI, -ClBrI)[8,12-17]. For instance, MXene with -O/-S terminations withstand 10,000 cycles at 10 A/g[15]. $Ti_3C_2T_x$ MXene with -OH/-O terminations achieves a gravimetric capacitance of 314 F/g via alkali treatment, outperforming HF-etched counterparts by roughly 214%[18], while n-butyllithium-treated $Ti_3C_2T_x$ MXenes obtain a capacitance of 523 F/g at 2 mV/s and retain 96% capacity after 10,000 cycles[19], partly due to the fact that more O-terminations increase the capacitance via proton bonding/debonding[19-21]. Despite progress, the atomistic mechanism linking termination (e.g., halogen) electronegativity to EDL capacitance remains unresolved[22].

In this work, we combine density functional theory (DFT) calculations (VASP/JDFTx) with systematic electrochemical characterization to resolve the mechanistic ambiguity surrounding halogen terminations' impact on capacitance.

EXPERIMENTAL

Materials

HCl (~37 wt%), HF (~40 wt%), hydrobromic acid (HBr, ~40 wt%), hydroiodic acid (HI 48-57 wt%), isopropyl alcohol (≥ 99.7%) and ethanol (99.5%) were obtained from Shanghai Hushi Laboratory Supplies Co., Ltd. Gallium metal (99.999%), Nafion perfluorinated resin solution was purchased from Shanghai Aladdin Biochemical Technology Co., Ltd. Molybdenum carbide (99.5%) was provided by Alfa Aesar (China) Chemical Co., Ltd. These reagents were used as received without further purification. Deionized water (DIW, resistivity > 18 MΩ·cm) was collected from a Milli-Q Biocel system.

Synthesis of Mo_2Ga_2C

Mo_2Ga_2C powder was prepared by mixing and sintering commercial Mo_2C powder with Ga, following the procedure reported in previous literature.

Synthesis of Mo_2CF_x

To prepare Mo_2CF_x MXene, 200 mg of Mo_2Ga_2C was slowly added to a 50 mL Teflon-lined autoclave. Subsequently, 20 mL of HF was gradually introduced into the autoclave and stirred for 5 min. The mixture was then left at room temperature for 5 days to facilitate the etching reaction. After reaction, the residual powder was washed with DIW and anhydrous ethanol until reaching a neutral pH. The powder was then freeze-dried for 24 h to obtain Mo_2CF_x.

Synthesis of Mo_2CT_x (T = Cl, Br, I)

To prepare Mo_2CT_x MXene, concentrated hydrohalic acid (HX) were used to purify Mo_2CF_x sample. In a typical procedure, 200 mg Mo_2CF_x was slowly added to a 50 mL Teflon-lined autoclave. Subsequently, 20 mL of concentrated HX (X = Cl, Br, I) acid was gradually introduced into the autoclave and stirred for 5 min. The mixture was then left at 180 ℃ for 1 day to facilitate the purification. After purification, the residual powder was washed with DIW and anhydrous ethanol until reaching a neutral pH. The powder was then freeze-dried for 24 h to obtain Mo_2CT_x.

RESULTS AND DISCUSSION

Theoretical calculations

Firstly, the structural models of partial Mo_2CT_x (T = F, Cl, Br, I) MXenes along the c-axis are presented in Figure 1A, with the yellow regions representing surface termination and the blue regions indicating the solvation areas. The enthalpy of formation for halogen-terminated Mo_2CT_x MXene was calculated [Figure 1B]. The enthalpies of formation for Mo_2CF_x, Mo_2CCl_x, Mo_2CBr_x, and Mo_2CI_x are -1.57, -0.93, -0.77, and -0.49 eV/atom, respectively. The bonding strength between terminations is F > Cl > Br > I, similar to the bonding strength of $Ti_3C_2T_x$ MXene surface terminations, suggesting that this order of bonding strength may be universally present in MXenes[8]. Figure 1C-F illustrates the density of states for Mo_2CT_x, indicating that all four types of Mo_2CT_x MXene are metallic in nature[23,24]. Mo_2CT_x MXene displays exceptional electrical conductivity, especially in the case of Mo_2CCl_x, Mo_2CBr_x, and Mo_2CI_x. The majority of electrons near the Fermi surface in Mo_2CT_x MXene are supplied by the Mo d-orbital electrons, followed by surface terminations[23,25]. For Mo_2CF_x, the Mo and C elements almost do not provide electrons, which might be the reason why the F terminations do not participate in redox reactions and thus display inert behavior[26,27]. However, for other Mo_2CT_x MXenes, the surface terminations provide electrons near the Fermi surface and thus generate additional redox peaks in the redox process, thereby increasing the capacity of the supercapacitor[17]. Hence, they are potential candidates for supercapacitors. Figure 1G shows the integral specific capacitance in the voltage window of -0.6 to 0.6 V *vs.* point of zero charge (PZC). The integral capacitances of Mo_2C with halogen terminations are 9.23, 10.10, 11.30, and 12.96 μF/cm², respectively. The order of the integral capacitance size is Mo_2CF_x < Mo_2CCl_x < Mo_2CBr_x < Mo_2CI_x.

Figure 1H shows the quantum capacitance (C_Q) of Mo_2CT_x (T = F, Cl, Br, I) MXene. Since Mo_2CF_x has the fewest electrons at the Fermi level, its C_Q at the Fermi level is also the smallest. The C_Q behavior of Mo_2CT_x MXene is completely different from that of graphene, which exhibits a "V" shape due to the Dirac point[28,29]. The C_Q of monolayer graphene is about 20 μF/cm² at 0.6 eV, while the minimum C_Q of Mo_2CT_x is 200 μF/cm², far greater than that of graphene[28]. The quantum charge curves in Figure 2A show that the quantum charging capacity of Mo_2CI_x is the smallest, indicating that the regulation of terminations can indeed effectively control the C_Q behavior of MXene.

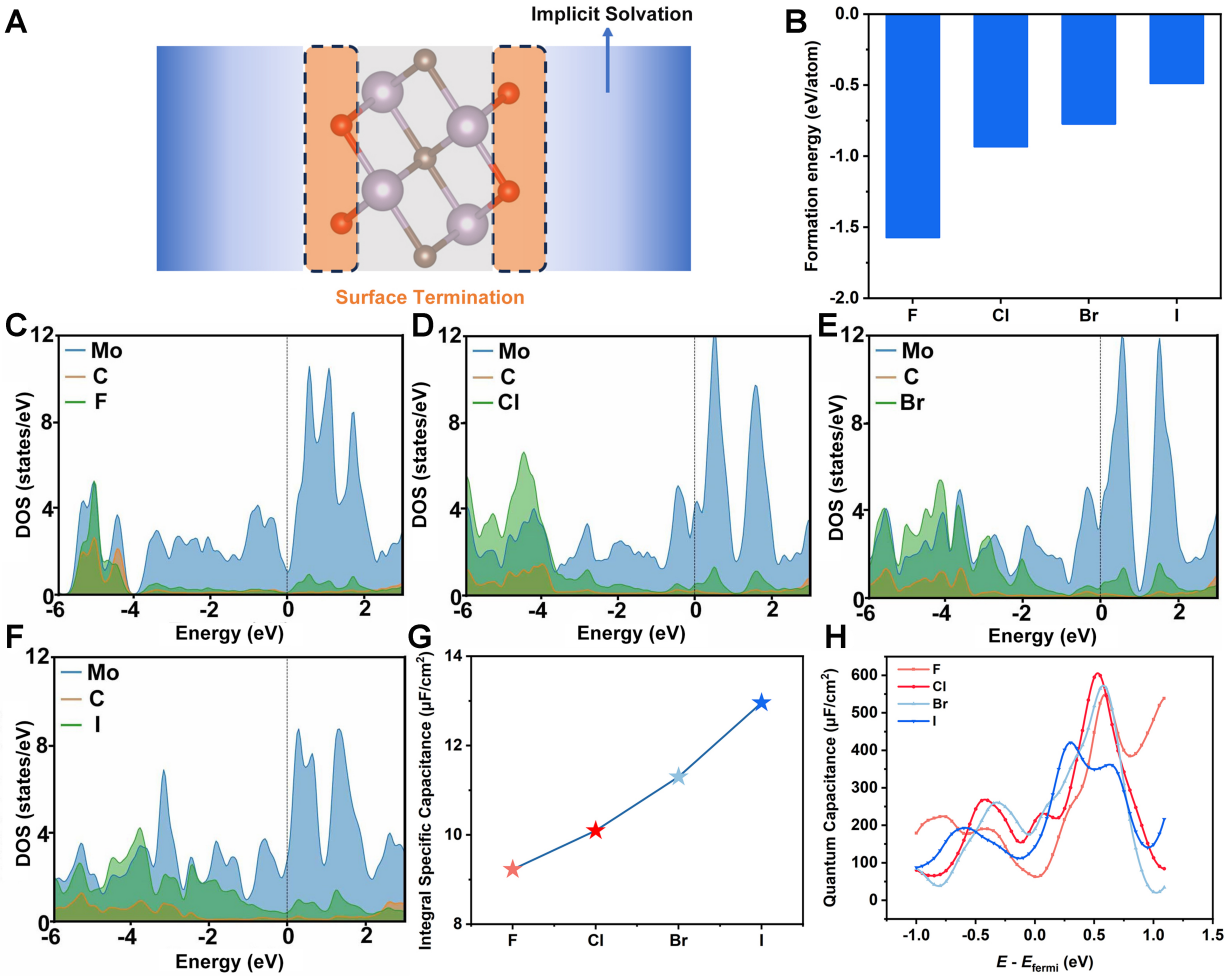

Figure 1. Structure, electronic, and capacitive properties of surface-terminated Mo_2CT_x (T = F, Cl, Br, I) MXene. (A) Structure model of Mo_2CT_x. The yellow area represents surface terminations, and the blue area represents the solvation region; (B) The formation energy of Mo_2CT_x; (C-F) The density of states of Mo_2CT_x; (G) Integral specific capacitance of Mo_2CT_x. The salmon, red, light-blue, and dark-blue stars represent Mo_2CF_x, Mo_2CCl_x, Mo_2CBr_x, and Mo_2CI_x, respectively; (H) C_Q of Mo_2CT_x. C_Q: Quantum capacitance; DOS: density of states.

To reveal the impact of terminations changes on EDL capacitance, the electronic structure of the EDL at the electrode/electrolyte interface was calculated. Figure 2B shows the net charge distribution of the electrode and the electrolyte along the z-direction at an applied potential of 1 V *vs.* PZC. Notably, most of the net charge exists at the electrode/electrolyte interface. As halogens belong to the same group, the distribution shape of the excess charge in both the electrode and the electrolyte is almost the same, indicating that the charge distribution shape is independent of the surface terminations. As the atomic radius increases, the positive center of the electrode and the negative center of the electrolyte gradually deviate from the surface. The thickness of the double layer can be obtained by calculating the difference between the two centers. Figure 2B shows that as the electronegativity decreases, the thickness of the double layer decreases. According to the definition of a parallel plate capacitor, capacitance is inversely proportional to thickness, so its capacitance increases, consistent with the EDL charge curves corresponding to Mo_2CT_x (T = F, Cl, Br, I) MXene calculated in Figure 2C. In order to better study the charge distribution on the electrode surface, differential electron densities between charged (1 V *vs.* PZC) and uncharged Mo_2CT_x MXene were calculated. Interestingly, most of the charge is distributed on the surface of terminations that directly contact the electrolyte, implying the termination's significant impact on the capacitance of MXene electrodes.

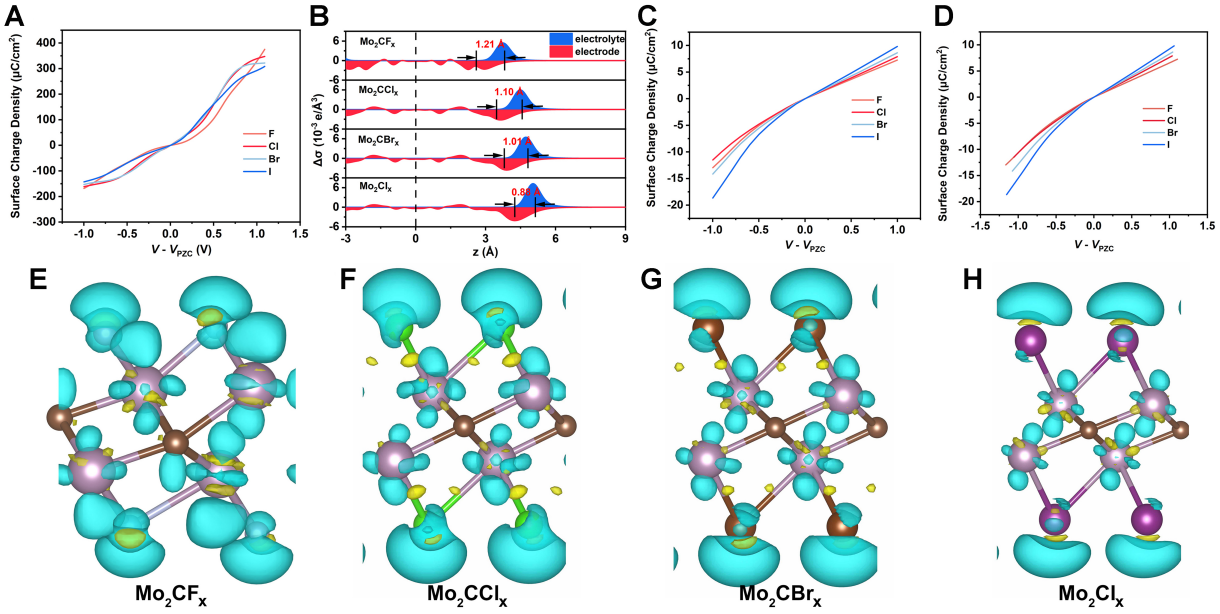

Figure 2. Charge distribution and electrical double layer characteristics of surface-terminated Mo_2CT_x (T = F, Cl, Br, I) MXenes. (A) Quantum charge curves corresponding to Mo_2CT_x; (B) Net charge distribution of electrode and electrolyte along the z direction, where the position of C layer is at z = 0 Å. The electrode applied potential is 1 V *vs.* PZC; (C) EDL charge curves corresponding to Mo_2CT_x; (D) Total charge curves corresponding to Mo_2CT_x; (E-H) Iso-surface (0.0005 e/Å^3) of differential electron densities between charged (1 V *vs.* PZC) and uncharged Mo_2CT_x. PZC: point of zero charge; EDL: electric double-layer.

The total capacitance C_{Tot} can be obtained by connecting the C_Q and the double-layer capacitance in series. Since C_{EDL} is much smaller than C_Q, the total capacitance is mainly determined by C_{EDL}. This is similar to metal electrodes[30]. From Figure 2D, it is found that whether at positive voltage or negative voltage, the total charge curve of Mo_2CF_x is the smallest, and Mo_2CI_x is the largest. The derivative of Figure 2D gives the differential capacitance of Mo_2CT_x MXene. Supplementary Figure 1 shows that when a positive voltage is applied, the differential capacitance of Mo_2CT_x is almost a constant, about 6-9.5 μF/cm². However, in the negative voltage region, the differential capacitance of Mo_2CI_x can be as high as 22 μF/cm². The differential capacitance of graphene is roughly 3-5 μF/cm²[28]. To probe charge redistribution at the electrode-electrolyte interface, differential electron density iso-surfaces (isovalue = 0.0005 e/Å^3) were calculated for charged (1 V *vs.* PZC) *vs.* uncharged Mo_2CT_x MXenes, shown in Figure 2E-H. Figure 2E (Mo_2CF_x) displays charge mainly on F terminations, indicating strong shielding from high electronegativity, restricting Mo electron delocalization. Figure 2F (Mo_2CCl_x) shows broader density on Cl, with reduced shielding. Figure 2G (Mo_2CBr_x) reveals increased localization on Br and Mo layers, boosting surface electrons. Figure 2H (Mo_2CI_x) exhibits the strongest accumulation on I and Mo, due to low electronegativity, thinning the EDL for better ion access. Overall, decreasing electronegativity from F to I enhances charge redistribution, matching the capacitance order and emphasizing terminations' role in MXene performance.

Based on the theoretical results, the capacitance behavior of Mo_2CT_x MXene can be effectively controlled through the regulation of terminations. Given that all Mo_2CT_x MXenes are metallic, their capacitance is primarily contributed by double-layer capacitance. When Mo_2C is modified by functional groups with smaller electronegativity, its total capacitance increases, primarily due to the weakening of electrostatic shielding, leading to a reduction in the double-layer thickness. Therefore, the capacitance order is Mo_2CF_x < Mo_2CCl_x < Mo_2CBr_x < Mo_2CI_x. This lays a foundation for understanding the electrochemical behavior of surface terminations of Mo_2CT_x MXene in capacitance.

Experimental verification

In order to further prove the theoretical claims, Mo_2CF_x samples prepared by HF etching were further purified using HCl, HBr, and HI through a solvothermal method to obtain samples with specific surface terminations. These four samples were named Mo_2CF_x, Mo_2CCl_x, Mo_2CBr_x and Mo_2CI_x. Furthermore, the specific preparation strategy is described in the Methods section. As shown in Figure 3A, after the exfoliation of Ga atomic layers, Mo_2CT_x (T = F, Cl, Br, I) exhibited similar X-ray diffraction (XRD) results. Compared to the Mo_2Ga_2C precursor, the (002) peak located at around 10° shifted to a lower angle. Besides, the intensities of the remaining diffraction peaks decreased significantly, indicating the successful preparation of MXene. Specifically, the XRD patterns show (002) peak positions at 8.52° for Mo_2CF_x, 8.76° for Mo_2CCl_x, 8.50° for Mo_2CBr_x, and 8.46° for Mo_2CI_x. This overall trend confirms progressive enlargement with decreasing halogen electronegativity and increasing atomic size from F to I, facilitating improved ion accessibility. The exception for Mo_2CCl_x (smaller d-spacing than Mo_2CF_x) can be attributed to incomplete drying of the Mo_2CF_x sample, leading to retained interlayer water that increases its spacing, while the post-processing for Mo_2CCl_x removes such water more effectively, resulting in a more compact structure. Scanning electron microscope (SEM) results reveal the typical layer structure after removed Ga layers [Supplementary Figure 2]. What is more, F, Cl, Br, I terminations are observed clearly via energy-dispersive X-ray spectroscopy (EDS) results [Supplementary Figure 3]. As depicted in Figure 3B, since Mo_2CCl_x, Mo_2CBr_x, and Mo_2CI_x were prepared by solvothermal purification based on Mo_2CF_x, the area ratios of the oxidation peaks Mo^{5+} and Mo^{6+} increased significantly compared to Mo_2CF_x, implying more pronounced surface oxidation. This can be attributed to the oxidizing properties of HCl, HBr, and HI, which promoted the oxidation process on the surface of Mo_2CF_x. During the solvothermal treatment, these acid molecules acted as oxidants, oxidizing Mo atoms to higher valence states of Mo^{6+} and Mo^{5+}, leading to an increase in the area ratio of these two valence states. In the solvothermal process, the F terminations on the surface of Mo_2CF_x were replaced by -Cl, -Br, or -I. As the electronegativity decreases in the order of Cl, Br, and I, the degree of electron cloud density shifting towards the Mo atoms in the covalent bonds formed with Mo increases accordingly. Consequently, the electron cloud density around the Mo atoms increases, shielding the effective positive charge experienced by the inner electrons and reducing the bond energy of Mo-C. In the X-ray photoelectron spectroscopy (XPS) survey spectrum [Figure 3C], the F terminations on the surface of the Mo_2CF_x sample were replaced by -Cl, -Br, and -I from the HCl, HBr, and HI solutions, respectively. This can be attributed to the solvothermal conditions providing sufficient energy and reaction environment to promote the nucleophilic attack of Cl^-, Br^-, and I^- on the Mo–F bonds, forming the corresponding termination. Intriguingly, the C 1s spectra and termination-specific spectra across the four samples collectively corroborate these conclusions [Supplementary Figures 4 and 5]. While the solvothermal halogen substitution process is designed to replace F with Cl, Br, or I, the subsequent washing with DIW and ethanol may introduce minor oxygen terminations (-O or -OH), as is typical in MXene post-processing. Any trace oxygen presence could marginally enhance pseudo-capacitive contributions (as discussed for -O/-OH in the Introduction), potentially slightly elevating measured capacitances beyond pure EDL effects. Nevertheless, the experimental capacitance hierarchy (Mo_2CF_x < Mo_2CCl_x < Mo_2CBr_x < Mo_2CI_x) aligns closely with DFT predictions for idealized pure-halogen models, indicating limited influence from oxygen on the overall trends.

Furthermore, compared to Mo_2CF_x, the Mo absorption edges of Mo_2CCl_x, Mo_2CBr_x, and Mo_2CI_x shifted significantly towards higher energies, which is consistent with the XPS results, indicating an increase in the valence state of Mo [Figure 3D]. The results of the Mo K-edge extended X-ray absorption fine structure (EXAFS) [Figure 3E] showed that the coordination numbers of Mo–Mo and Mo–C at 2.5 and 1.5 Å followed the order of Mo_2CI_x > Mo_2CBr_x > Mo_2CCl_x > Mo_2CF_x (without fitting). It is evident that due to the electronegativity order of -F > -Cl > -Br > -I, stronger electronegativity leads to stronger covalency and shorter bond lengths, resulting in increased distances between adjacent Mo atoms and weakened interactions between Mo atoms and Mo as well as C. Consequently, the coordination number of Mo decreases with

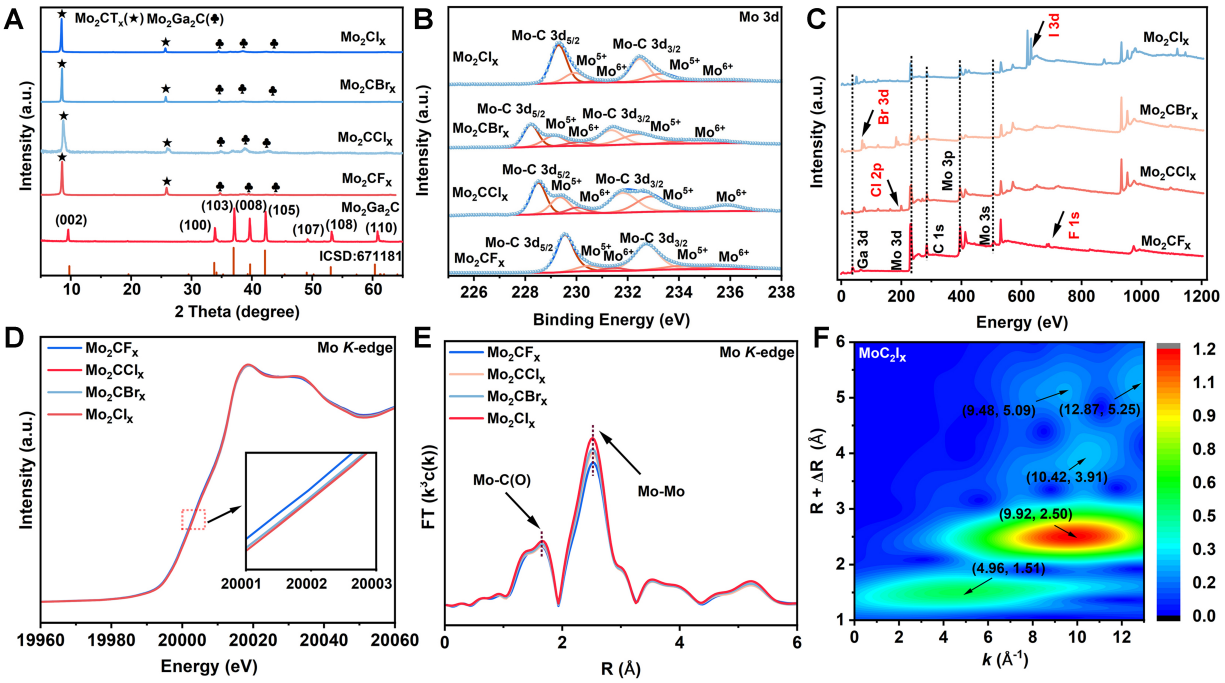

Figure 3. Spectroscopic analysis of the structure of surface-terminated Mo_2CT_x (T = F, Cl, Br, I) MXene. (A) XRD patterns; (B) XPS spectrum of Mo 3d; (C) XPS full spectrum; (D) Normalized XANES spectra of Mo K-edge; (E) FT-EXAFS of Mo K-edge; (F) WT of Mo_2Cl_x. XRD: X-ray diffraction; XPS: X-ray photoelectron spectroscopy; XANES: X-ray absorption near-edge structure; FT-EXAFS: Fourier-transformed extended X-ray absorption fine structure; WT: wavelet transform.

increasing electronegativity of the termination. In the wavelet transform (WT) results [Figure 3F and Supplementary Figure 6], two maxima were observed at around 9.9 and 4.9 Å, corresponding to the chemical bonding environments of Mo–Mo and Mo–C, respectively. In summary, through systematic characterization analysis, it was confirmed that the solvothermal method can effectively control the surface terminations composition of Mo_2CT_x MXene. More importantly, the electronegativity of different terminations significantly affects the structural and electronic properties of the material, such as Mo valence state, Mo–C bond energy, and the coordination environments of Mo–Mo and Mo–C. These results provide important experimental evidence for understanding the structure-property relationship of MXene materials.

To further explore the influence of different surface terminations on the electrochemical performance of MXene materials, Mo_2CT_x (T = F, Cl, Br, I) was used as thin-film electrodes for supercapacitors. The experiments were conducted in 1 M H_2SO_4 electrolytes. As shown in Figure 4A-D, no obvious redox peaks appeared for the four samples at different scan rates, indicating that the electrochemical behavior of the samples was mainly non-Faradaic capacitance. The quasi-rectangular CV shape indicates fast pseudo-capacitive kinetics, where diffusion-controlled intercalation dominates without discrete peaks, as is typical in MXenes[13,20]. The cyclic voltammetry (CV) curves of the four samples at different scan rates exhibited similar shapes, suggesting that the capacitance behavior had a weak dependence on the scan rate, implying good rate performance, electrochemical stability, and fast charge-discharge capability of the samples. The rapid charge storage and release can be achieved precisely because the charge storage primarily occurs on the electrode surface, and the charge transfer and diffusion paths are short, while the layered structure of MXene provides a structurally stable framework for charge storage. Importantly, at the same scan rate, the area enclosed by the CV curves follows the order of Mo_2CI_x > Mo_2CBr_x > Mo_2CCl_x > Mo_2CF_x, suggesting that the terminations I with lower electronegativity and larger size is beneficial for the adsorption and desorption of electrolyte ions, enhancing the EDL capacitance effect.

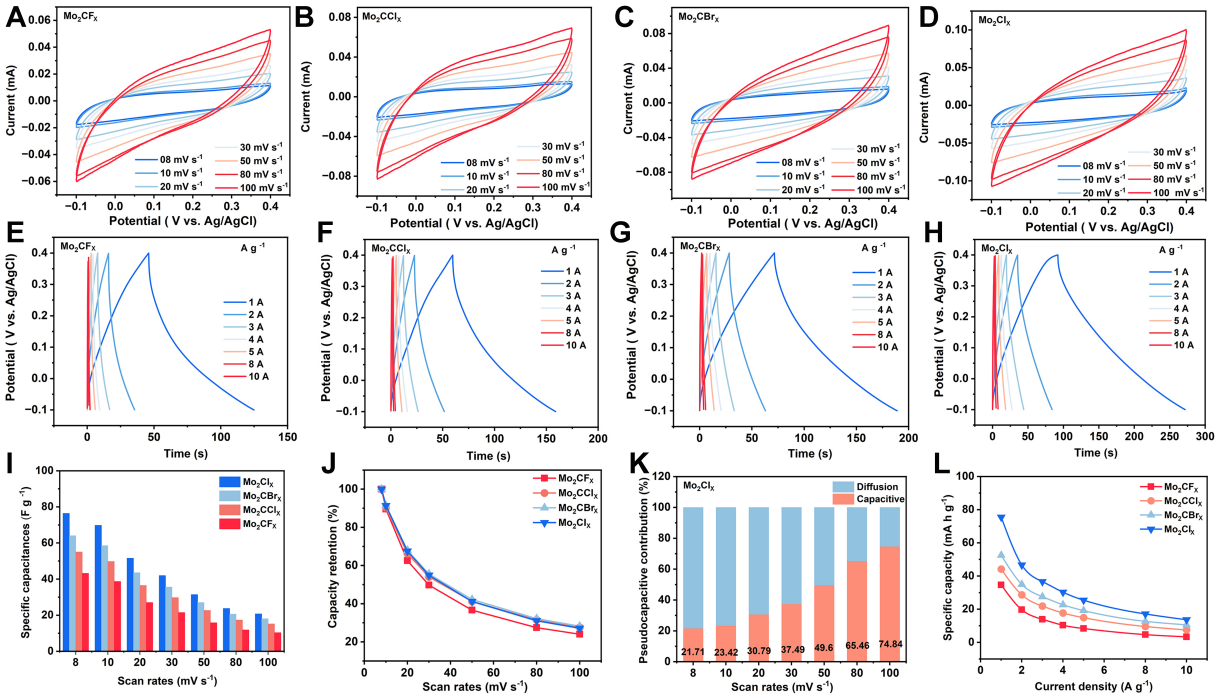

Figure 4. Electrochemical performance of surface-terminated Mo_2CT_x (T = F, Cl, Br, I) MXene. (A-D) The CV curves of Mo_2CT_x electrodes at different scan rates; (E-H) The GCD curves of Mo_2CT_x electrodes at different scan rates; (I) Capacitance comparison of the Mo_2CT_x electrode at different scan rates; (J) Capacitance retention at different scan rates; (K) The calculated diffusion and capacitive ratios at different scan rates for Mo_2CI_x; (L) Capacitance comparison of the Mo_2CT_x electrode at different current densities. CV: Cyclic voltammetry; GCD: galvanostatic charge/discharge.

As shown in Figure 4E-H, the galvanostatic charge/discharge (GCD) curves of the four samples Mo_2CF_x, Mo_2CCl_x, Mo_2CBr_x, Mo_2CI_x were measured at different current densities. At the same current density, the charge-discharge time of the samples follows the order of Mo_2CI_x > Mo_2CBr_x > Mo_2CCl_x > Mo_2CF_x. Longer charge-discharge times corresponding to higher specific capacitances. This sequence can be attributed to the terminations I with lower electronegativity, which leads to a higher electron cloud density on the surface Mo atoms of MXene and a lower EDL thickness, making it more favorable for the adsorption and desorption of electrolyte ions and enhancing the EDL capacitance effect. Despite a slight decrease in the overlap of the GCD curves at high currents, the shape of the GCD curves for all four samples remained highly consistent across multiple currents, demonstrating the excellent stability of the materials. No significant decay in charge-discharge time or severe deformation of the curve shape was observed during the cycling process, suggesting that the electrode materials can maintain their structural integrity and electrochemical activity during the charge-discharge process. This stability can be attributed to the unique layered structure of MXene and the regulation of the structural and electronic properties of the materials by surface terminations modification. The specific capacitances and capacitance retention rates of Mo_2CT_x (T = F, Cl, Br, I) samples at different scan rates are summarized in Figure 4I and J. As seen, the Mo_2CI_x sample achieves the highest specific capacitance of 76.3 F/g at a scan rate of 8 mV/s. Overall, the specific capacitances of the samples at various scan rates follow the order of Mo_2CI_x > Mo_2CBr_x > Mo_2CCl_x > Mo_2CF_x. Moreover, as the scan rate increases, Mo_2CI_x consistently maintains the highest capacitance retention rate. The capacitive contribution analysis reveals a self-adaptive dual-mode mechanism in Mo_2CT_x MXene [Figure 4K and Supplementary Figure 7]. At low scan rates, diffusion-controlled behavior dominates, analogous to battery-type ion intercalation, while high-rate operation shifts overwhelmingly to capacitance dominated kinetics. This transition originates from MXene's distinctive 2D layer architecture, which provides exceptionally high specific surface area and abundant active sites for rapid surface redox reactions and modulated ion-transport pathways through interlayer galleries, further enhanced by surface functional group participation in Faradaic

processes. Figure 4L illustrates the specific capacitances of the four samples at different current densities. Remarkably, Mo_2CI_x attains an impressive specific capacitance of 74.9 mA·h/g (539.3 F/g) at a current density of 1 A/g, which is 1.35 times that of Mo_2CBr_x, 1.66 times that of Mo_2CCl_x, and 2.16 times that of Mo_2CF_x at the same current density. Similarly, as the current density continues to increase, the specific capacitance gradually decreases.

Through the above systematic electrochemical performance measurements, we confirmed that the Mo_2CT_x (T = F, Cl, Br, I) samples have a charge storage mechanism dominated by non-Faradaic capacitance. The electronegativity and size of different terminations have significant effects on the electrochemical performance. Combining the results of structural analysis, the I termination with lower electronegativity and larger size can result in increasing the electron cloud density of the surface Mo atoms of MXene, reducing the EDL thickness, and increasing the specific surface area and active sites of the materials. These results reveal the intrinsic correlation between the structure and performance of MXene materials and are consistent with our theoretical calculations, may provide useful guidance for the design and optimization of high-performance MXene electrode materials.

CONCLUSIONS

In this work, we integrated theoretical calculations and experimental investigations to elucidate the regulatory effect of halogen terminations on the electrochemical performance of Mo_2CT_x MXenes for supercapacitor applications. The simulations revealed that the capacitance of halogen-terminated Mo_2CT_x MXenes is primarily contributed by the EDL capacitance, which can be effectively tuned by modifying the surface terminations. The total capacitance increased as the electronegativity of the terminations decreased, following the order of Mo_2CF_x < Mo_2CCl_x < Mo_2CBr_x < Mo_2CI_x. Experimental results further validated the theoretical predictions, confirming that the I termination in Mo_2CT_x with lower electronegativity and larger size could enhance the EDL capacitance effect and increases the specific capacitance. These findings provide valuable insights into the intrinsic correlation between the structure and performance of MXene, facilitating the rational design and optimization of high-performance MXene electrode materials for advanced supercapacitors.

DECLARATIONS

Acknowledgments

We thank the Beijing Synchrotron Radiation Facility (1W1B), Hefei Synchrotron Radiation Facility (Infrared spectroscopy and microspectroscopy, MCD-A and MCD-B, Photoemission and Catalysis/Surface Science), and USTC Center for Micro and Nanoscale Research and Fabrication for helps in characterizations. Computational work was performed at the Hefei Advanced Computing Center. The AI-driven experiments, simulations and model training were performed on the robotic AI-Scientist platform of Chinese Academy of Science.

Authors' contributions

Made substantial contributions to the experimental design and execution: Xu, H.
Made substantial contributions to the computational design and execution: Shou, H.
Contributed to data analysis and interpretation and led the manuscript writing: Xu, H.; Shou, H.
Provided guidance for the computational study: Zhou, Q.; Liu, H.; Wei, S.; Wu, X.; Wang, C.; Song, L.
Provided scientific guidance and supervision, administered the project, and acquired funding: Wu, X.; Wang, C.; Song, L.
Contributed to scientific discussion and manuscript revision: Xu, H.; Shou, H.; Zhou, Q.; Liu, H.; Wei, S.; Wu, X.; Wang, C.; Song, L.
Approved the final version of the manuscript: Xu, H.; Shou, H.; Zhou, Q.; Liu, H.; Wei, S.; Wu, X.; Wang, C.; Song, L.

Availability of data and materials

The raw data supporting the findings of this study are available within this Article and its Supplementary Materials. Further data are available from the corresponding authors upon request.

AI and AI-assisted tools statement

During the preparation of this manuscript, the AI tool OpenAI ChatGPT (version GPT-5, released 2025-08-07) was used solely for language editing. The tool did not influence the study design, data collection, analysis, interpretation, or the scientific content of the work. All authors take full responsibility for the accuracy, integrity, and final content of the manuscript.

Financial support and sponsorship

We extend our gratitude for the financial support received from the National Key R&D Program of China (2022YFA1504104 and 2022YFA1605400), NSFC (12225508, U23A20121, 22075264, and 22225301), the Strategic Priority Research Program of the Chinese Academy of Sciences (XDA0410401) and the Fundamental Research Funds for the Central Universities (WK2060000099, 20720220009, and WK2490000001) and USTC Bihe Youth Program for Interdisciplinary Innovation (BH-202508).

Conflicts of interest

All authors declared that there are no conflicts of interest.

Ethical approval and consent to participate

Not applicable.

Consent for publication

Not applicable.

Supplementary Materials

Supplementary Materials

REFERENCES

1. VahidMohammadi, A.; Rosen, J.; Gogotsi, Y. The world of two-dimensional carbides and nitrides (MXenes). *Science* **2021**, *372*, eabf1581. DOI PubMed
2. Wang, D.; Zhou, C.; Filatov, A. S.; et al. Direct synthesis and chemical vapor deposition of 2D carbide and nitride MXenes. *Science* **2023**, *379*, 1242-7. DOI PubMed
3. Lim, K. R. G.; Shekhirev, M.; Wyatt, B. C.; Anasori, B.; Gogotsi, Y.; Seh, Z. W. Fundamentals of MXene synthesis. *Nat. Synth.* **2022**, *1*, 601-14. DOI
4. Liu, J.; Cao, H.; Jiang, B.; Xue, Y.; Fu, L. Newborn 2D materials for flexible energy conversion and storage. *Sci. China. Mater.* **2016**, *59*, 459-74. DOI
5. Chen, X.; Paul, R.; Dai, L. Carbon-based supercapacitors for efficient energy storage. *Natl. Sci. Rev.* **2017**, *4*, 453-89. DOI
6. Hu, M.; Dai, J.; Chen, L.; et al. Selectivity for intercalated ions in MXene toward a high-performance capacitive electrode. *Sci. China. Mater.* **2023**, *66*, 974-81. DOI
7. Kajiyama, S.; Szabova, L.; Iinuma, H.; et al. Enhanced Li-ion accessibility in MXene titanium carbide by steric chloride termination. *Adv. Energy. Mater.* **2017**, *7*, 1601873. DOI
8. Li, M.; Li, X.; Qin, G.; et al. Halogenated Ti_3C_2 MXenes with electrochemically active terminals for high-performance zinc ion batteries. *ACS. Nano.* **2021**, *15*, 1077-85. DOI PubMed
9. Zheng, C.; Yao, Y.; Rui, X.; et al. Functional MXene-based materials for next-generation rechargeable batteries. *Adv. Mater.* **2022**, *34*, e2204988. DOI PubMed
10. Ghidiu, M.; Lukatskaya, M. R.; Zhao, M. Q.; Gogotsi, Y.; Barsoum, M. W. Conductive two-dimensional titanium carbide 'clay' with high volumetric capacitance. *Nature* **2014**, *516*, 78-81. DOI PubMed
11. Dall'agnese, Y.; Lukatskaya, M. R.; Cook, K. M.; Taberna, P.; Gogotsi, Y.; Simon, P. High capacitance of surface-modified 2D titanium carbide in acidic electrolyte. *Electrochem. Commun.* **2014**, *48*, 118-22. DOI

12. Zhang, P.; Shou, H.; Xia, Y.; et al. X-ray insights into formation of -O functional groups on MXenes: two-step dehydrogenation of adsorbed water. *Nano. Lett.* **2023**, *23*, 1401-8. DOI PubMed
13. Li, Y.; Shao, H.; Lin, Z.; et al. A general Lewis acidic etching route for preparing MXenes with enhanced electrochemical performance in non-aqueous electrolyte. *Nat. Mater.* **2020**, *19*, 894-9. DOI PubMed
14. Li, M.; Lu, J.; Luo, K.; et al. Element replacement approach by reaction with Lewis acidic molten salts to synthesize nanolaminated MAX phases and MXenes. *J. Am. Chem. Soc.* **2019**, *141*, 4730-7. DOI PubMed
15. Shen, M.; Jiang, W.; Liang, K.; et al. One-pot green process to synthesize MXene with controllable surface terminations using molten salts. *Angew. Chem. Int. Ed. Engl.* **2021**, *60*, 27013-8. DOI PubMed
16. Kamysbayev, V.; Filatov, A. S.; Hu, H.; et al. Covalent surface modifications and superconductivity of two-dimensional metal carbide MXenes. *Science* **2020**, *369*, 979-83. DOI PubMed
17. Jawaid, A.; Hassan, A.; Neher, G.; et al. Halogen etch of Ti_3AlC_2 MAX phase for MXene fabrication. *ACS. Nano.* **2021**, *15*, 2771-7. DOI PubMed
18. Li, T.; Yao, L.; Liu, Q.; et al. Fluorine-free synthesis of high-purity $Ti_3C_2T_x$ (T=OH, O) via alkali treatment. *Angew. Chem. Int. Ed. Engl.* **2018**, *57*, 6115-9. DOI PubMed
19. Chen, X.; Zhu, Y.; Zhang, M.; et al. *N*-butyllithium-treated $Ti_3C_2T_x$ MXene with excellent pseudocapacitor performance. *ACS. Nano.* **2019**, *13*, 9449-56. DOI PubMed
20. Lukatskaya, M. R.; Bak, S.; Yu, X.; Yang, X.; Barsoum, M. W.; Gogotsi, Y. Probing the mechanism of high capacitance in 2D titanium carbide using *in situ* X-ray absorption spectroscopy. *Adv. Energy. Mater.* **2015**, *5*, 1500589. DOI
21. Zhan, C.; Naguib, M.; Lukatskaya, M.; Kent, P. R. C.; Gogotsi, Y.; Jiang, D. E. Understanding the MXene pseudocapacitance. *J. Phys. Chem. Lett.* **2018**, *9*, 1223-8. DOI PubMed
22. Jing, C.; Tao, S.; Fu, B.; et al. Layered double hydroxide-based nanomaterials for supercapacitors and batteries: strategies and mechanisms. *Prog. Mater. Sci.* **2025**, *150*, 101410. DOI
23. Gan, J.; Li, F.; Tang, Y.; Tang, Q. Theoretical study of transition-metal-modified Mo_2CO_2 MXene as a catalyst for the hydrogen evolution reaction. *ChemSusChem* **2020**, *13*, 6005-15. DOI PubMed
24. Zhang, J. J.; Dong, S. Superconductivity of monolayer Mo_2C: the key role of functional groups. *J. Chem. Phys.* **2017**, *146*, 034705. DOI PubMed
25. Shimada, T.; Takenaka, N.; Ando, Y.; Otani, M.; Okubo, M.; Yamada, A. Relationship between electric double-layer structure of MXene electrode and its surface functional groups. *Chem. Mater.* **2022**, *34*, 2069-75. DOI
26. Wang, C.; Shou, H.; Chen, S.; et al. HCl-based hydrothermal etching strategy toward fluoride-free MXenes. *Adv. Mater.* **2021**, *33*, e2101015. DOI PubMed
27. Kotmool, K.; Kaewmaraya, T.; Hussain, T.; Ahuja, R.; Luo, W.; Bovornratanaraks, T. Biaxial stress and functional groups (T = O, F, and Cl) tuning the structural, mechanical, and electronic properties of monolayer molybdenum carbide. *Phys. Chem. Chem. Phys.* **2022**, *24*, 17862-9. DOI
28. Zhan, C.; Neal, J.; Wu, J.; Jiang, D. Quantum effects on the capacitance of graphene-based electrodes. *J. Phys. Chem. C.* **2015**, *119*, 22297-303. DOI
29. Zhan, C.; Jiang, D. E. Contribution of dielectric screening to the total capacitance of few-layer graphene electrodes. *J. Phys. Chem. Lett.* **2016**, *7*, 789-94. DOI PubMed
30. Li, C. Y.; Le, J. B.; Wang, Y. H.; et al. *In situ* probing electrified interfacial water structures at atomically flat surfaces. *Nat. Mater.* **2019**, *18*, 697-701. DOI PubMed